Research Article **IJNR (2017) 1:3**

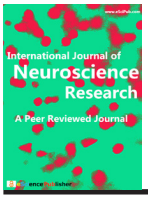

International Journal of Neuroscience Research
(ISSN:2572-8385)

Autophagy Is Up Regulated In A Neuronal Model Of Charcot-Marie Tooth Disease That Overexpresses Dynamin 2 Mutant

Anu Shanu[1, 3, 5] Scott E. Stimpson[1, 3, 4] Jens R. Coorssen[†2,3,4,5] and Simon J. Myers[†1,3,4,5]

Western Sydney University,[1]Neuro-Cell Biology Laboratory, [2]Molecular Physiology, [3]Molecular Medicine Research Group, [4]School of Science and Health, [5]School of Medicine, Locked Bag 1797, NSW 2751, Australia

ABSTRACT

Dominant-Intermediate Charcot-Marie-Tooth disease is one of the most common inherited disorders affecting the peripheral nervous system. Pleckstrin homology domain mutations in dynamin 2 cause dominant-intermediate Charcot Marie Tooth Syndrome. Autophagy in normal cells helps to maintain homeostasis and degrade damaged or old organelles and proteins. Here we link the pleckstrin homology domain mutants and the disease state to autophagy. Cells over-expressing the K558E mutation in the pleckstrin homology domain of dynamin 2 have shown an increase in expression of ER stress and autophagy markers. Although the exact link between autophagy and peripheral neurodegeneration has yet to be fully elucidated, these results set the foundation for further research into the interactions between dynamin 2 mutations, autophagy, and Dominant-Intermediate Charcot-Marie-Tooth.

Keywords:
DI-CMT, Dynamin II, autophagy, autophagosome.

How to cite this article:
Shanu et al.,. Autophagy Is Up Regulated In A Neuronal Model Of Charcot-Marie Tooth Disease That Overexpresses Dynamin 2 Mutant. International Journal of Neuroscience Research, 2017; 1:3.

***Correspondence to Author:**
Dr. Simon Myers [To communicate with Editorial and Production Offices] Address: Western Sydney University, Office 21.1.05, Campbelltown campus, Locked Bag 1797, Penrith, NSW 2751, Australia Phone: +61 02 4620 3383 Email: s.myers @uws.edu.au Facsimile: +61 4620 3025;

Professor Jens Coorssen
Address: Dean, Faculty of Graduate Studies, Brock University, Niagara Region. 1812 Sir Isaac Brock Way, St Catharines, Ontario. L2S3A1. Canada, Phone: 9056885550 x5346, Email:jcoorssen @brocku.ca Facsimile: 9053785705.

eSciencePublisher
eSciPub LLC, Houston, TX USA.
Website: http://escipub.com/

I. Introduction

Dominant-Intermediate Charcot-Marie-Tooth disease (DI-CMT), also known as hereditary motor and sensory neuropathy, is one of the most common inherited neurologic disorders (Liu *et. al.,* 2014). DI-CMT presents in the first to second decade of life with distal muscle weakness and sensory impairment. DI-CMT is characterised by reduced nerve conduction velocity due to loss of the myelin sheath.

Missense mutations within the Dynamin 2 (DNM2) locus, K558E, cause DI-CMT (Zuchner *et. al.,* 2005). DNM2 is a ubiquitously expressed effector protein and is part of the dynamin superfamily (Praefcke and McMahon, 2004). All classical dynamins share the same structure, consisting of a GTPase domain (GD), middle domain (MD), pleckstrin homology domain (PH), GTPase effector domain (GED) and a Proline-Rich domain (PRD). Of the known mutations, the majority occur within the PH domain of DNM2, which may impair its lipid binding ability, thus potentially affecting its membrane association. Structural studies of the PH domain of DNM2 indicate that the residues affected in DI-CMT are part of β3/ β4 loop that mediates interaction with the acyl chain of phosphoinositides (Zuchner *et. al.,* 2005). Thus, reduced DNM2 membrane binding capacity and an altered cellular distribution may contribute to the pathological mechanism of DI-CMT neuropathies.

DNM2 is recruited to sites of vesicle scission via protein-lipid interactions mediated by the PRD and PH domains. GTP hydrolysis results in a conformational change, and DNM2 forms a collar around the neck of a vesicle in the terminal stages of endocytosis (Praefcke and McMahon, 2004). The DNM2 collar then constricts and pinches the tubular membrane neck, completing fission of the endocytotic vesicle from the plasma membrane (Ramachandran, 2010). DNM2 has also been shown to directly interact with the microtubule and actin cytoskeletal network thus mediating trafficking of intracellular cargo via the fission of budding vesicles (McNiven *et al.,* 2005). It has been observed that in central nervous system (CNS) neuropathies presenting with axonal degenerations, autophagy is upregulated (Jaeger and Wyss-Coray, 2009). Whether similar effects are observed in peripheral sensory (PNS) neuropathies also presenting with axonal degenerations remains unclear.

Endoplasmic reticulum (ER) is the principal system in the cell that senses the presence of unfolded/ misfolded mutant proteins and initiate mechanisms to improve the stress that ensues, via chaperone proteins such as calnexin. Sustained imbalance of ER homeostasis leads to ER stress, which activates the unfolded protein response (UPR) that culminates in autophagy (Yin *et. al.,* 2016). This is instigated by three effector proteins: PKR-like eukaryotic initiation factor 2α kinase (PERK) and inositol requiring enzyme 1 (IRE1), which are both protein kinases, and activating transcription factor 6 (ATF6); all reside in the ER lumen, in an inactive state. Upon aggregation of unfolded proteins, or other ER stressor factors, these proteins are activated initiating a complex signalling pathway that results in autophagy (Malhotra & Kaufman, 2011). Autophagy is the lysosomal pathway that carries out the degradation of cytoplasmic materials and organelles (Ghavami *et. al.,* 2014). A basal level of autophagy helps maintain cellular homeostasis by eliminating old and damaged organelles and thus enhancing protein turnover (Ghavami *et. al.,* 2014). Upon the initiation of autophagy, a phagophore is formed via an isolation membrane surrounding the damaged organelle and associated cytosol, which then undergoes elongation until it seals itself, forming an autophagosome (AP) (Ghavami *et. al.,* 2014). MAP1LC3 is a specific marker for AP and is anchored via conjugated phosphatidylethanolamine (MAP1LC3-II) to the isolation membrane (Jaeger and Wyss-Coray, 2009). AP formation is dependent on the products of autophagy related genes (ATG) (Klinosky *et. al.,* 2003: Yorimitsu and Klinosky, 2005). Once formed, AP fuses to a late endosome or multi-vesicular body to form an amphisome, and subsequently to a lysosome to form an autolysosome and is further subjected to degradation by lysosomal hydrolases and, finally, cargo sorting (Ghavami *et. al.,* 2014). Detailed mechanisms and the core machinery involved in each stage of autophagosome formation, maturation and degradation are discussed elsewhere (Codogno *et. al.,* 2014).

In this study, we have begun to elucidate the molecular pathways leading to DNM2 mutation associated neurodegeneration in the context of

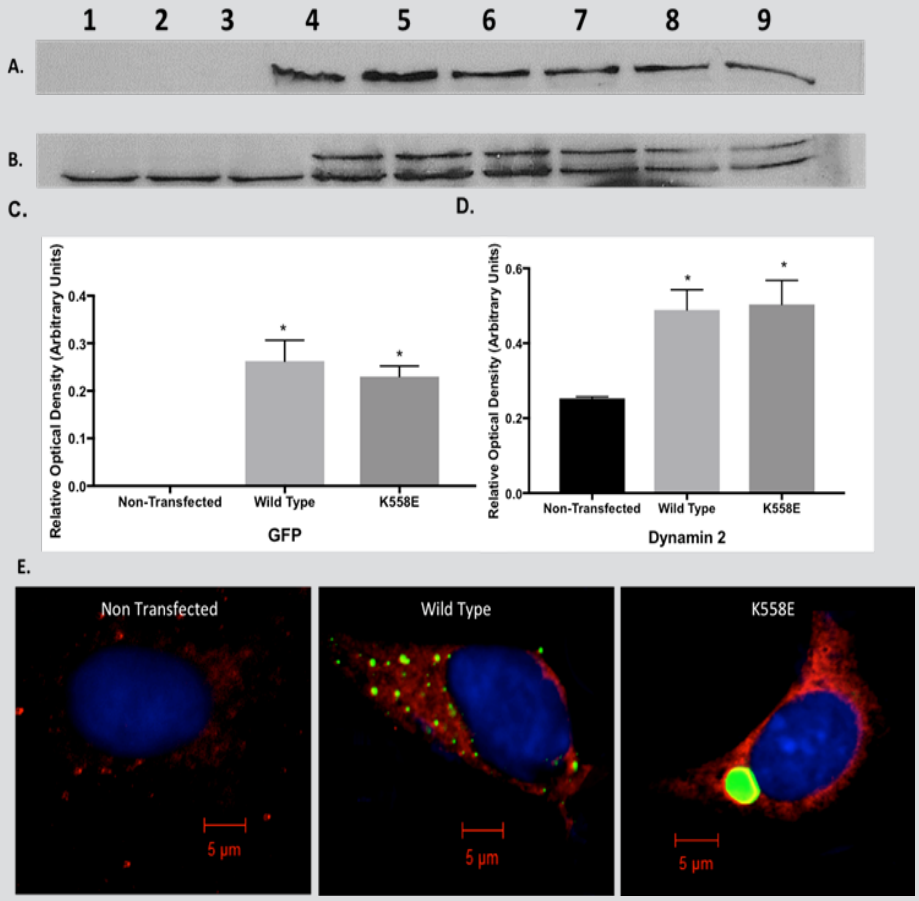

Figure 1: Characterizing dynamin transfection in SH-SY5Y neuroblastoma cells. A) Immunoblot detection of GFP (B) Immunoblot detection of Dynamin-2. Lanes 1 -3 represents NT SH-SY5Y total proteins, 4-6 represents WT SH-SY5Y total proteins, 7-9 represents K558E SH-SY5Y total proteins. (C and D) A representative graph showing statistically significant difference between NT, WT and K558E of GFP (p <0.005) and Dynamin-2 (p <0.05) respectively (n=3). Blots normalised to GAPDH. Errors bar depict SE of means. (E) Representative confocal micrographs showing NT, WT and K558E Dynamin-2 stained SH-SY5Y (red), GFP (green) and DAPI nuclear stain (blue). Scale bar = 5 µm.

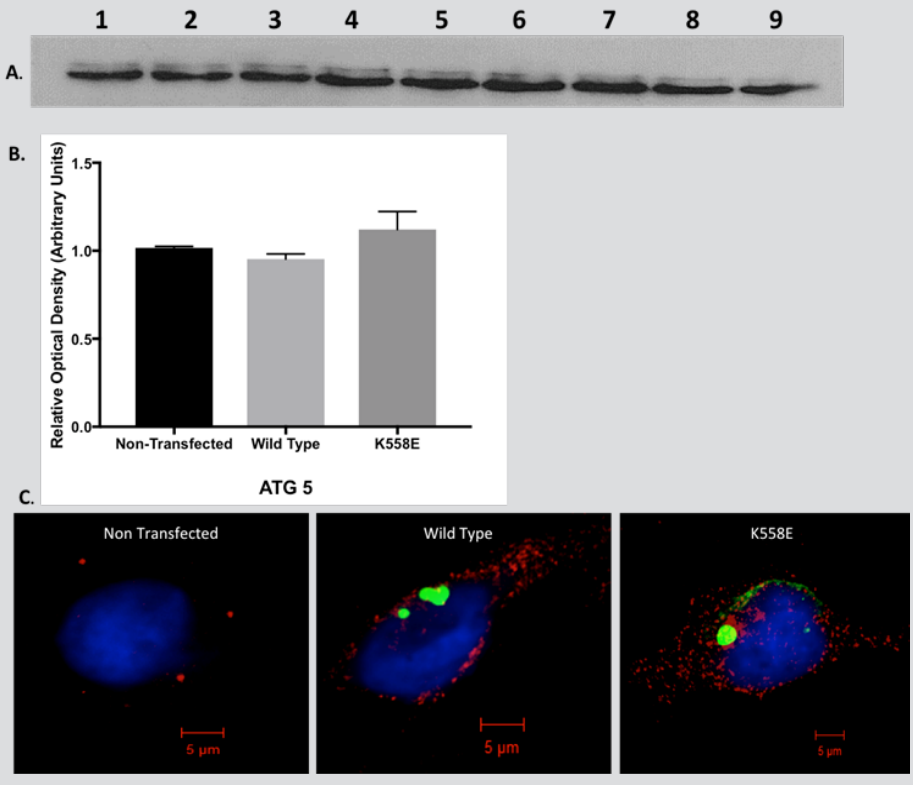

Figure 2: Detection of ATG5 in DNM2 mutant neuronal cells. A) Immunoblot detection of ATG5. Lanes 1 -3 represents NT SH-SY5Y total proteins, 4-6 represents WT SH-SY5Y total proteins, 7-9 represents K558E SH-SY5Y total proteins. (B) A representative graph showing no statistical significant difference between NT, WT and K558E of ATG5 (n=3). Blot normalised to GAPDH. Errors bar depict SE of means. (E) Representative confocal micrographs showing NT, WT and K558E ATG5 stained SH-SY5Y (red), GFP (green) and DAPI nuclear stain (blue). Scale bar = 5 µm.

enhanced ER stress and autophagy. Our studies show a significant increase in expression of autophagy and autophagosome markers in cells over-expressing the wild type and K558E mutant of DNM2. Not surprisingly, we also saw an increase in ER stress marker calnexin in the cells expressing the K558E mutant. These findings emphasize the linkage between DNM2 mutations and ER stress mediated autophagy, and may further enable the identification of potential critical mechanisms underlying DI-CMT.

II. Results

Characterizing transient transfection in SH-SY5Y neuroblastoma cells: SH-SY5Y neuroblastoma cells were transiently transfected (TT) with DNM2 containing either the wild type (WT) or the K558E PH domain mutant tagged with GFP. Quantitative analysis of the immunoblots (Figure 1C and 1D) and immunofluorescence analysis (Figure 1E) confirmed that transfection enhanced the expression levels of total DNM2, with transfected DNM2 appearing as higher molecular weight band compared to the endogenous DNM2 (Figure 1B).

Intracellular localisation of DNM2 and autophagy proteins within transiently transfected SH-SY5Y cells: The intracellular localisation and abundance of the proteins DNM2, ATG5, ATG12, Beclin-1, LCB I and II were established using immunostained TT SH-SY5Y cells expressing NT, WT and mutant K558E. There were no apparent changes in intracellular localisation of the DNM2 when transfected with GFP labelled DNM2, with both the native and labelled proteins localising to the cell periphery and cytoplasm (Figure 1E). ATG5 and ATG12 are both involved in the expansion of the phagophore; when unconjugated they reside within the cytoplasm or a preautophagosomal membrane structure within the cytoplasm. Both ATG5 and ATG12 displayed a consistent cytoplasmic pattern throughout the cell in NT, WT and mutant (Figures 2C and 3C). Beclin-1 is classically found to be distributed throughout the cytoplasm, mitochondrial membrane and Golgi. Beclin-1 displayed an even distribution throughout the WT and mutant cells (Figure 4C). LC3B I and II were distributed evenly throughout the cytoplasm of the cells, indicating no change in the localisation within the WT and mutant cells compared to the NT cells (Figure 5D).

Expression of autophagy proteins within transiently transfected SH-SY5Y cells: To determine the expression of autophagy, total cellular protein fractions from NT, WT and mutant K558E TT SH-SY5Y cells were isolated and quantitative immunoblot analyses were carried out (Figures 1A, 1B, 2A-5A). Quantitation of immunoblots from NT, WT and mutant SH-SY5Y cells revealed no statistically significant ($p > 0.05$) changes in expression of ATG5 and Beclin 1 (Figure 2B, 4B). However, K558E mutants showed a significant increase in ATG12 ($p < 0.01$, Figure 3B), LC3B I and II expression ($p < 0.01$; Figure 5 B and C), and WT cells showed significant increase in ATG12 ($p < 0.01$; Figure 3B), LC3B I and II expression ($p < 0.001$; Figure 5B and C) compared to that seen in NT cells. An increased presence of acidic vacuolar organelles (AVO) was further confirmed in WT and mutant cells using acridine orange (AO) staining to visualize assessment these punctate structures (Figure 6A). This was further confirmed by flow cytometry, establishing a 1.4-fold increase in AVOs in Wild type cells, a 1.5-fold increase in K558E expressing cells, and 4.2-fold increase in serum starved cells (Figure 6B, 6C).

Expression of ER proteins within transiently transfected SH-SY5Y cells: To assess the effect of the mutations on basal ER protein expression, immunoblotting was used to detect the molecular chaperone calnexin and ER kinase PERK, which are both indicators of autophagy following ER stress (Figure 7A, B). K558E cells showed a significant increase in calnexin compared to both NT and WT cells ($p < 0.005$) (Figure 7C). Calnexin was not upregulated in WT cells. The ER kinase PERK was however found to be increased in both WT and K558E expressing cells ($p < 0.01$) (Figure 7D). This was accompanied by a mobility shift of the WT and mutant bands (lanes 4-9) indicating activation of PERK by phosphorylation, as phosphorylated PERK shows slightly lower mobility compared to the non-phosphorylated protein (Kumar *et. al.,* 2001).

Mitochondrial proteins and metabolism: Mitochondrially encoded cytochrome c oxidase II (MTCO2), a mitochondrial marker, was measured by immunoblotting to assess modulations in post-transfection protein levels, which revealed no significant change between the groups (Fig-

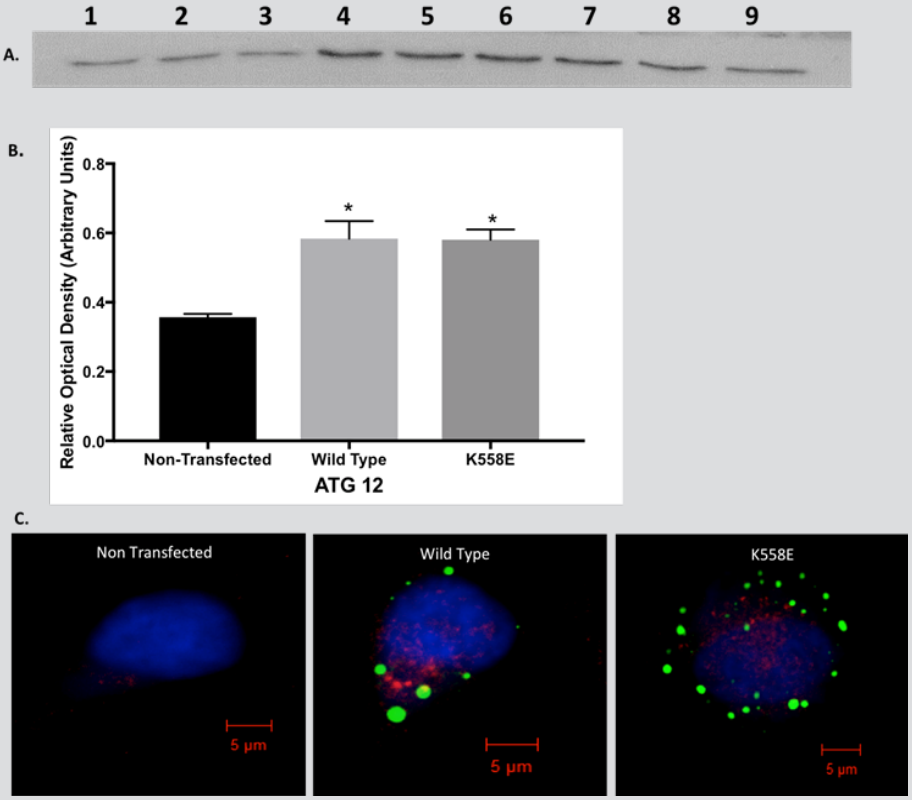

Figure 3: Detection of ATG12 in DNM2 mutant neuronal cells. A) Immunoblot detection of ATG12. Lanes 1 -3 represents NT SH-SY5Y total proteins, 4-6 represents WT SH-SY5Y total proteins, 7-9 represents K558E SH-SY5Y total proteins. (B) A representative graph showing statistically significant ($p < 0.01$) difference between NT, WT and K558E of ATG12 (n=3). Blot normalised to GAPDH. Errors bar depict SE of means. (E) Representative confocal micrographs showing NT, WT and K558E ATG12 stained SH-SY5Y (red), GFP (green) and DAPI nuclear stain (blue). Scale bar = 5 µm.

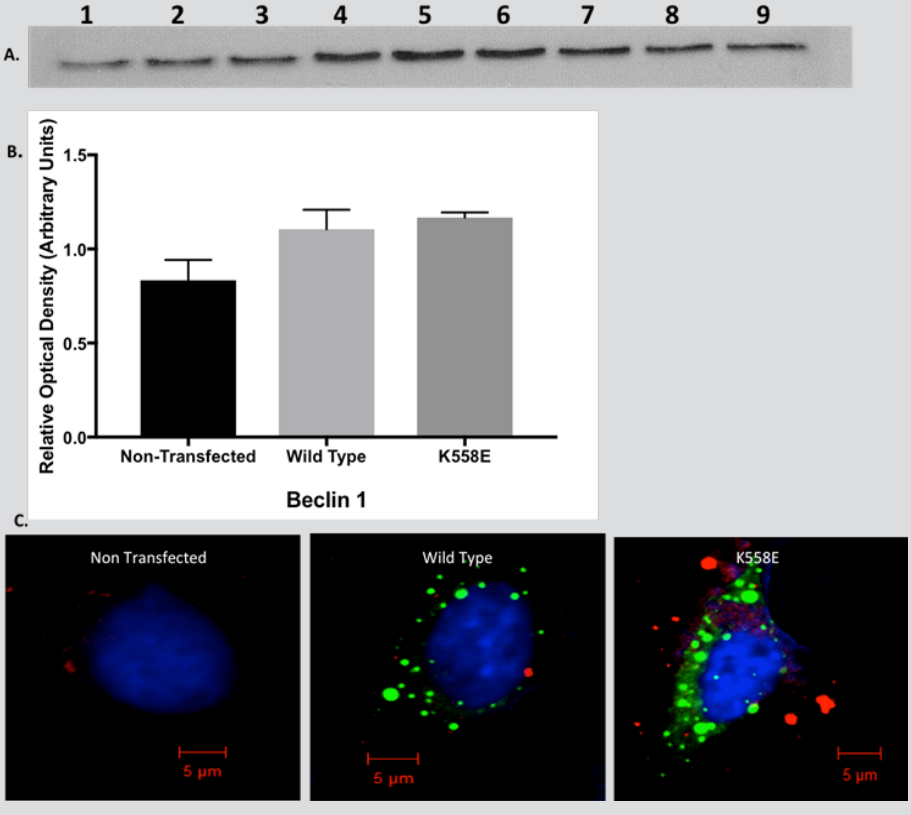

Figure 4: Detection of Beclin-1 in DNM2 mutant neuronal cells. A) Immunoblot detection of Beclin-1. Lanes 1 -3 represents NT SH-SY5Y total proteins, 4-6 represents WT SH-SY5Y total proteins, 7-9 represents K558E SH-SY5Y proteins. (B) Graph showing no significant difference between the cells (n=3). Blot normalised to GAPDH. Errors bar depict SE of means. (E) Representative confocal micrographs showing NT, WT and K558E Beclin-1 stained SH-SY5Y (red), GFP (green) and DAPI nuclear stain (blue). Scale bar = 5 µm.

ure 8A, B). Monitoring of cellular ATP levels also did not show any significant change between the transfected cells compared to the non-transfected cells (Figure 8C).

Receptor mediated endocytosis: Transferrin intake was measured by quantifying the uptake of transferrin-conjugated with Texas Red, as a means to measure RME. Overall, K558E mutant showed a marked decrease in transferrin uptake compared to NT and WT ($p < 0.005$) (Figure 9A). This was also evident in the images of cells stained by transferrin-Texas Red, in which punctate structures were distinctly visible in NT and WT groups but only detectable to a much lower extent in K558E cells (Figure 9B).

III. Discussion

Removal of Schwann cells (SC) causing demyelination, is a common characteristic of DI-CMT, having a negative effect on nerve conduction velocities in DI-CMT patients (Claeys *et al.,* 2009). With autophagy potentially an element of this disease, two possible explanations can be inferred. Firstly, that autophagy may be playing a positive role in cleaning up neuronal and protein aggregates (Jaeger and Wyss-Coray, 2009; Lee, 2009) and second, that autophagy is increased in response to nerve remyelination with SC. It has been shown that activation of autophagy aides in nerve remyelination (Rangarajy *et al.,* 2010). As such the demyelinated axons could be a cause for the up regulation of autophagy and may be linked to the neuronal repair and remyelination processes. Along with the demyelination of neurons, the degeneration of axons is also a hallmark of DI-CMT. While the link between autophagy and such axonal degeneration is well established in the CNS (Ferguson *et. al.,* 2009; Koch *et al.,* 2010; Ghavami *et. al.,* 2014), no such mechanistic relationship has been described within the PNS.

The data presented establish that SH-SY5Y cells transfected with K558E mutants undergo unfolded protein mediated ER stress, which potentially acts as a contributing factor to the progression of autophagy in DI-CMT. Autophagy is driven by a set of more than 30 ATG proteins including Beclin 1 (ATG 6), along with other specialised proteins such as Class 3 phosphoinositide-3-kinase (PIK3C3) that form the core machinery which recruits the isolation membrane and drives it through elongation and maturation steps (Yin *et. al.,* 2016*)*. The elongation phase results in formation of double-membrane autophagosome, which requires the complex formation of ATG5-ATG12 proteins in addition to other autophagic proteins, and finally formation of mature autophagosomes. This complex is also responsible for enlisting microtubule-associated protein light chain-3 (LC3) which is cleaved by ATG4 protease to form LC3 I and is further conjugated with phosphatidylethanolamine to form LC3 II, which are both markers for mature autophagosomes (Kirkin *et. al.,* 2009). Upon fusion with lysosomes to form the autolysosome, which is a type of acidic vacuolar organelle (AVO), LC3 II is dissociated from the membrane and is degraded. The process of autophagosome formation takes 5-10 min in mammals (Fujita *et. al.,* 2008) and hence the abundance of any of these proteins at any point of time is indicative of the stage of autophagy in the cells. In order to determine if autophagy were upregulated in TT SH-SY5Y cells over expressing the DNM2 K558E mutation, we quantitatively assessed the expression of proteins specific for autophagy. The over-expression of wild type DNM2 or the K558E mutant resulted in statistically significant increases in the expression of ATG12, LC3B I and II compared to NT cells. Increased expression of these markers is indicative of the up regulation of autophagy, while a decreased expression of these markers has shown to reflect impaired autophagy (Wu *et al.*, 2005; Kang *et al.*, 2011). Beclin 1 and ATG5 also showed a slight increase in the K558E group; whilst the increase observed was not statistically significant, the overall increase of the autophagy proteins within cells overexpressing the K558E mutant along with increased calnexin and activation of ER kinase, PERK, conclusively indicates that ER stress-mediated autophagy has a role in the progression of DI-CMT. Furthermore, immunofluorescence studies on the autophagy markers ATG12, ATG5, Beclin-1 and LC3B II and I have shown that there is considerable increase in the expression of these proteins in cells also expressing the DNM2 K558E mutation.

The successful execution of autophagy culminates with acidic hydrolysis of autolysosomal contents and release of the metabolites for recycling and/ or signalling (Nixon AR, 2013). Recent assessment of a dynamin mutant in *Drosophila* revealed autophagic dysfunction caused by

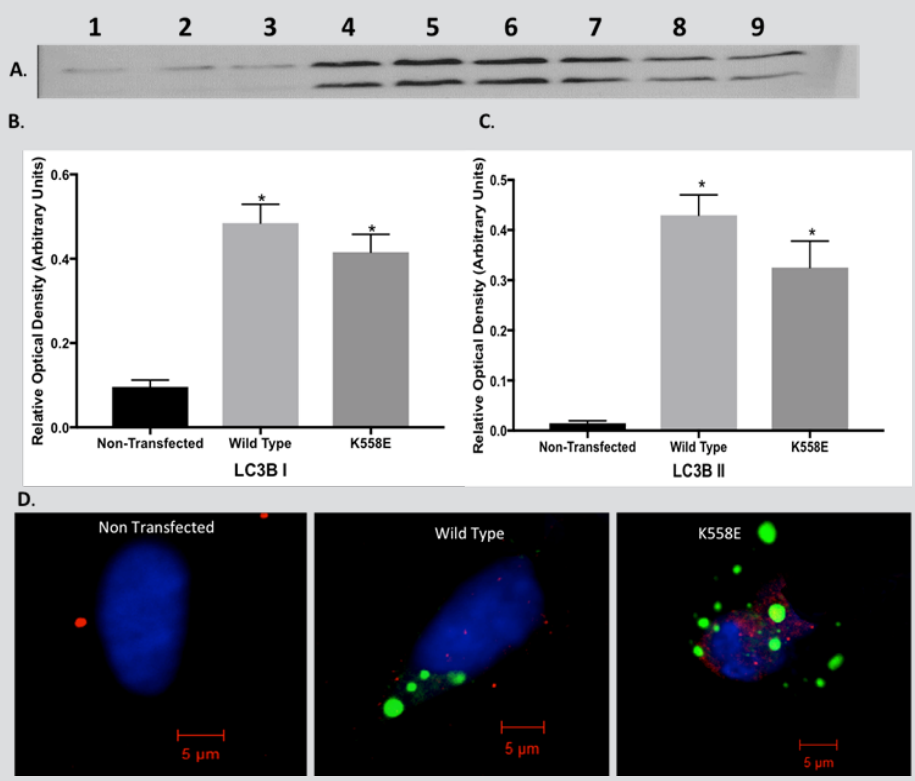

Figure 5: Detection of LC3B I and II in DNM2 mutant neuronal cells. A) Immunoblot detection of LC3B I and II. Lanes 1 -3 represents NT SH-SY5Y total proteins, 4-6 represents WT SH-SY5Y total proteins, 7-9 represents K558E SH-SY5Y total proteins. (C and D) A representative graph showing statistically significant ($p < 0.005$) difference between NT, WT and K558E of LC3B I and II respectively (n=3). Blots normalised to GAPDH. Errors bar depict SE of means. (E) Representative confocal micrographs showing NT, WT and K558E LC3B stained SH-SY5Y (red), GFP (green) and DAPI nuclear stain (blue). Scale bar = 5 µm.

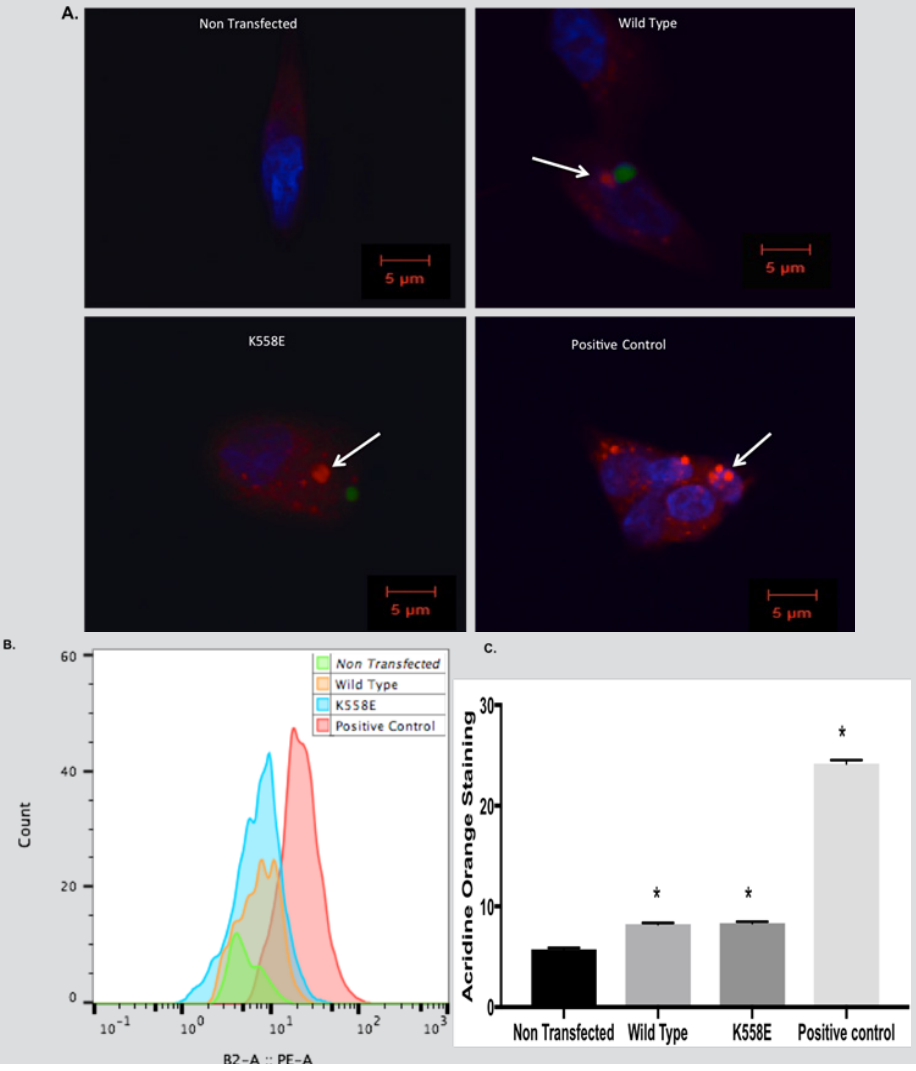

Figure 6: Acidic vacuolar staining in DNM2 mutant neuronal cells. Acridine orange staining was used to monitor acidic vacuolar organelles (white arrows) in non-transfected, wild type, DNM2 mutant and serum starved cells as positive controls. Representative confocal micrographs showing punctate structures (red), GFP-Dynamin (green) and DAPI nuclear stain (blue), n= 15. Scale bar = 5 µm. Flow cytometry was used to quantitate the increase in AVOs in different groups and shown as histograms in panel B with the analysis in panel C, showing significant increase in AVO staining in the transfected cells $p < 0.0001$.

defects in lysosomal acidification (Fang *et. al.,* 2016). An earlier study in DNM2 R465W mutant mice has also suggested impaired autophagy as a result of compromised function of vesicles, as a mechanism of pathogenesis of centronuclear myopathy (Durieux *et. al.,* 2012). However, in our hands, autophagic flux was found to be increased along the pathway, from the increased presence of autophagosomes to acidified autolysosomes.

Increased autophagy in the cells can be attributed to one or more reasons: a) as a mechanism to clear up aggregates of unfolded / mutated proteins, following signalling via increased ER-stress (Cai *et. al.,* 2016); b) as a counter strategy for decreased receptor mediated endocytosis (RME) to maintain cellular pools of essential resources (Hennig *et. al.,* 2006); c) nutrient starvation during which unwanted proteins are recycled in an attempt to maintain the cellular resource pool (Shang *et. al.,* 2011); or d) to simply reduce the protein overload as a result of overexpression of the DNM2 proteins (Nixon RA, 2012).

Indeed, K558E mutant cells show an increase in calnexin protein levels, indicating elevated ER stress as a result of unfolded protein aggregation. Furthermore, PERK, the ER kinase enzyme that initiates autophagy, was also found to be phosphorylated, confirming activation of autophagy. Up regulation of autophagy as a mechanism to offset reduced RME is also another possibility. Protein overload as a result of overexpression of transfected proteins may also contribute to the increase in autophagic flux. It is also be worth noting that some studies have found impaired autophagy as a result of dysfunctional dynamin proteins and subsequent impairment in membrane scission, which is in contrast to our results (Fang *et. al.,* 2016; Durieux *et. al.,* 2012). However, this could also be a possibility in our experiments if unfolded protein aggregates initiate autophagy but the pathway cannot be advanced due to dysfunctional transfected DNM2. However, it would seem that the endogenous copy of DNM2 compensates for this and enabling formation and maturation of autophagosome. A knockout model for DNM2 would be required to test this possibiliy, however, the stability of a DNM2 knock out model is questionable (Ferguson *et. al.,* 2009).

It was also interesting to note that there was increased expression of autophagic markers and AVOs in DNM2 wild type overexpressing cells. As there was no increase in calnexin levels or decrease in endocytosis, this could most probably be associated with increased protein load as a result of overexpression of DNM2, which initiates autophagic pathways.

Autophagy is known to play positive roles in neurodegenerative diseases, destroying [mutant?] cytoskeletal proteins along with degenerating organelles and aggregated proteins (Koch *et. al.,* 2010). Autophagy also helps maintain homeostasis within healthy neurons, thus aiding in suppression of neurodegeneration (Yue *et. al.,* 2009). Perhaps over time patients expressing the DNM2 K558E mutation have a sustained [up-]regulation of autophagy that can eventually trigger neuronal death. This would certainly be consistent with the prolonged nature of the disease.

The data presented here established that autophagy is upregulated in neuronal cells expressing the DNM2 K558E mutation and may play a role in the pathogenesis of DI-CMT. While further studies into the disease process and progression need to be undertaken, this work provides important insight to the molecular mechanisms involved, allowing for further studies into role(s) of autophagy in DI-CMT and other peripheral neuropathies.

IV. Materials

All cell culture stock solutions, including DMEM, Foetal Bovine Serum (FBS), Penicillin (100 U/ mL), Streptomycin (100 µg/ mL), L-glutamine (2 M), NEAA (1 M), and phosphate buffered saline (PBS) were purchased from GIBCO Invitrogen (Australia). Cell culture consumables were purchased from BD Falcon (Greiner, USA). MTCO2, PERK and GAPDH primary antibodies were purchased from Abcam (USA). Autophagy antibodies were purchased from Cell Signalling (USA). GFP primary antibodies were purchased from Merck Millipore (USA). Secondary horseradish peroxidase (HRP) rabbit antibodies, Acridine orange, glucose free media, D- galactose and DAPI stains were purchased from Sigma-Aldrich (Australia). Transferrin-texas red was purchased from Rockland Immunochemicals. And mitochondrial toxglo kit from Promega was used

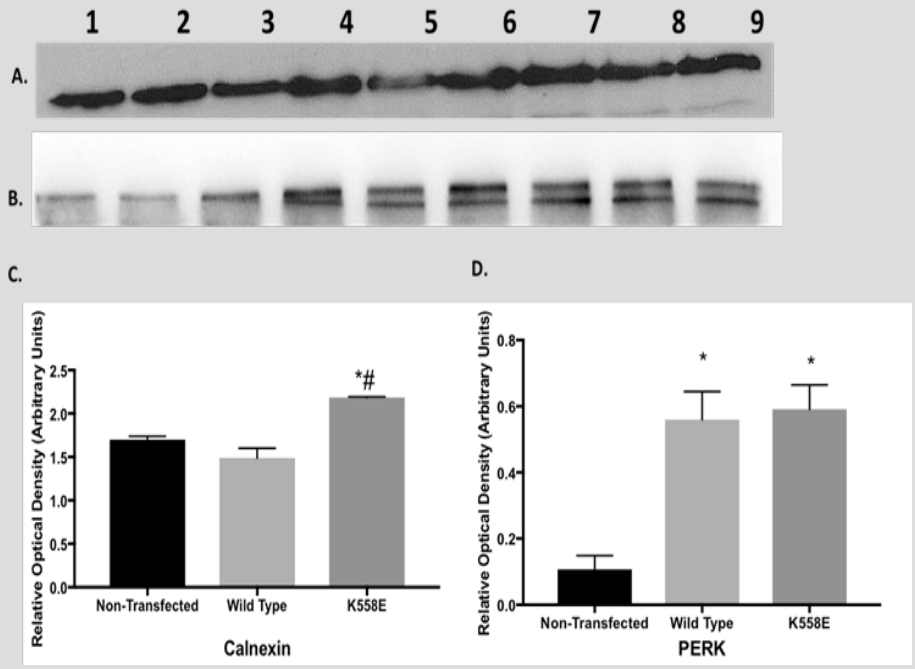

Figure 7: Expression of ER proteins in SH-SY5Y neuroblastoma cells. Expression of ER proteins Calnexin (A) and PERK (B) was detected using immunoblotting. Lanes 1 -3 represents NT, 4-6 represents WT, and 7-9 represents K558E proteins. Graphs showing relative expression of calnexin (C) and total PERK (D) in NT, WT and K558E mutants. Blots normalised to GAPDH. Error bar depict SE of means. (n=3). * Statistically significant increase compared to NT; # statistically significant increase compared to WT $p < 0.005$.

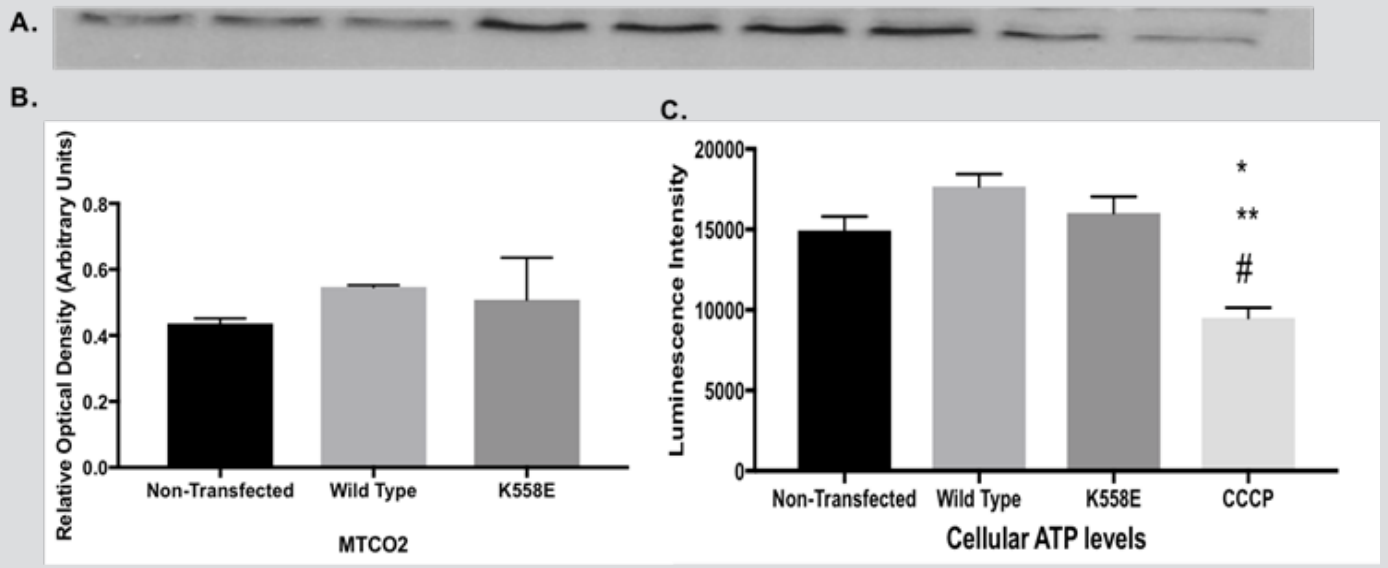

Figure 8: Mitochondrial marker MTCO2 and cellular ATP levels. Expression of mitochondrial cytochrome oxidase II (MTCO2) in NT, WT and mutant groups were detected using immunoblotting (A) and was quantitatively expressed (B). Lanes 1 -3 represents NT, 4-6 represents WT, and 7-9 represents K558E proteins. Blots normalised to GAPDH. Error bar depict SE of means. (n=3). Cellular ATP levels were also detected by measuring luminescence after addition of ATP detection mix containing enzyme luciferase and corresponding substrate luciferin (n=8). No significant change in cellular ATP levels was observed. CCCP was used as positive control. * Significant decrease vs NT; $p< 0.005$. ** significant decrease vs K558E # Significant decrease vs NT; $p< 0.005$.

to detect cellular ATP levels.

V. Methods

SH-SY5Y Cultures: SH-SY5Y cell lines were cultured in DMEM media (GIBCO), supplemented with FBS (10 % v/ v), Penicillin (1 U/ mL), Streptomycin (1 µg/ mL), L-glutamine (2 mM), and NEAA (1 mM) at 37 ^{o}C in a humidified atmosphere of 5 % CO_2, using T75 cm^2 culture flasks (Greiner, Interpath). Prior to use in biochemical assays, SH-SY5Ys were collected by centrifugation at 1,500 x *g* (5 min at RT) and washed in PBS. Cell counts were obtained using the Countess Automated Cell Counter (Invitrogen, Australia).

Transient Transfection: SH-SY5Y cells were TT with plasmid constructs (GFP-DNM2 WT and GFP-DNM2 K558E) using Lipofectamine 2000 (L2K; Invitrogen, USA). Cells were plated at a density of $2x10^5$ per well in 6 well plate. Transfections were carried out as per manufacturer instructions with 4 µg DNA and 5 µL L2K per well. Post transfection, the cells were incubated at 37 ^{o}C in a humidified atmosphere of 5 % CO_2 for 6 h. Cells then had media replaced with fresh media and were left to incubate for 48 h before harvesting for various analyses.

Protein Concentration: Determination of total cellular protein was performed using the EZQ Protein Estimation Assay (Invitrogen, Australia) as previously described by Churchward *et. al.,* (2005).

SDS-PAGE and Immunoblotting: NT, WT and K558E mutant fractions (25 µg total protein) were subjected to SDS-PAGE on 12.5% resolving gels and transferred to PVDF membranes. Non-reduced samples were used to detect total-PERK proteins, to specifically tag phosphorylated proteins. The membranes were blocked with 5% skim milk in TBS buffer containing 0.1% Tween-20. Membranes were incubated with anti-DNM2, anti-GAPDH, anti-MTCO2, anti-ATG5, anti-ATG12, anti-Beclin-1, anti-LC3B, anti-GFP, anti-PERK and anti-Calnexin antibodies at 1:1000, for 16 h. The membrane was then washed and incubated with secondary HRP antibody (1:2000 dilution) for 1 h at RT. Blots were developed using an enhanced chemiluminescence (ECL) detection kit (Pierce Thermo Scientific, USA). The membrane was developed on CL-Xposure Film (Thermo Fisher Scientific, U.S.A) using an AGFA X-ray developer. The signal intensities were measured using densitometry (ImageJ) and analysed using Graphpad Prism.

Immunofluorescence: Immunofluorescence was carried out as previously described by Stimpson *et. al.,* (2014). Briefly, SH-SY5Y cells ($1x10^6$ cells) were grown on glass coverslips in 6-well plates 24 h prior to transfection. 48 h post transfection, cells were washed with PBS and fixed with 4% paraformaldehyde. Cells were then permeabilised in 0.5% TritonX-100 at 37 ^{o}C for 30 min. The cells were blocked in 5% BSA solution at 37 ^{o}C for 30 min, followed by addition of primary antibody for DNM2, ATG5, ATG12, Beclin-1, LC3B and stained for 1 h at RT. The cells were subsequently washed and treated with secondary antibody, (anti-rabbit Rhodamine, Millipore, 1:200), and incubated for 1 h at RT. DAPI (1µg/ µL) was added for 2 min, the cells were washed twice with PBS. The coverslips were left overnight to dry and mounted onto glass slides prior to confocal imaging using the LSM 5 confocal microscope comprising the LSM 5 exciter laser scanning microscope with Axiovert 200M inverted optical microscope (Carl Zeiss, Jena, Germany).

Acridine Orange staining for acidic vacuolar organelles (AVOs): Transfected cells were seeded on glass coverslips in 6-well plates, 24 h post transfection and left overnight. NT cells serum starved for 6 h was used as positive controls. Prior to staining, cells were washed twice with PBS and incubated in AO at a final concentration of 1 µg / mL in HBSS and incubated at 37 ^{o}C for 15 min. Cells were washed twice, and fixed with 4% paraformaldehyde for 10 min. Cells were stained with DAPI and subsequently mounted on onto glass slides prior to confocal imaging using the LSM 5 confocal microscope (Ex. 488 nm; Em. 620 nm) comprising the LSM 5 exciter laser scanning microscope with Axiovert 200M inverted optical microscope (Carl Zeiss, Jena, Germany). Flow cytometric analysis was performed to measure acridine orange staining of AVOs. Cells were transfected in 6-well plates and incubated for 24 h. NT cells serum starved for 6 h was used as positive controls. Cells were washed in PBS, stained with AO (1 µg / mL HBSS) for 15 min at 37ºC, harvested and washed in PBS. Cells were resuspended in HBSS and immediately counted

using the MACSQuant flow cytometer (Miltenyi Biotech, Germany). Analysis was performed using Flowjo software.

Detection of Cellular ATP levels: Cellular ATP levels were detected using Mitochondrial Toxglo kit supplied by Promega, according to manufacturers instructions. 24 h post transfection, cells were reseeded onto opaque, white 96 well plates with 2.5×10^4 cells per well, and left overnight. Before experiment, the cells were washed with PBS and 100 µl of glucose free media containing 10mM galactose and 25 mM HEPES was added per well and incubated for 1 h. To this, 100 µL ATPase reagent (2X) was added, the plate was shaken (1 min) after which the luminescence signal was measured using a plate reader (BMG Fluostar Omega). CCCP was used as positive control.

Transferrin uptake assay: 24 h post transfection, cells were seeded either on glass coverslips in 6- well plates for microscopic analysis or black- walled 96-well plates (approx. 2.5×10^4 cells per well) for measurement of fluorescence intensity. Prior to staining, cells were washed with PBS and treated with 2 µg / mL for microscopy and 4 µg / mL for spectrometric analysis, for 30 min at 37 °C. Cells for microscopy were washed with PBS, fixed with 4% paraformaldehyde and stained with DAPI before mounting on glass slides for viewing under the LSM 5 confocal microscope (Ex. 595 nm; Em. 620 nm). Cells for spectrometric analysis were washed in PBS after staining, and measured using a plate reader (BMG Fluostar Omega). The wells were then washed with PBS and total protein per well was measured using BCA assay (Smith *et. al.,* 1985) and used to normalise the fluorescence reading.

Statistical Analysis: GraphPad Prism 7 was used for all statistical analyses. Data are reported as means ± S.E.M. Groups were compared by one-way ANOVA followed by the Tukey post hoc test with at least $p < 0.05$ considered statistically significant.

Acknowledgements

SJM and JRC acknowledge financial support from Miltenyi Biotec. We are grateful to Prof Phil Robinson (Cell Signalling Unit, Children's Medical Research Institute Sydney) for generously providing the GFP-DNM2 vector constructs used in this study. AS acknowledges funding from WSU MMRG Seed Grant for this project. SES was supported by an APA Research Scholarship, and the WSU School of Science and Health Postgraduate research fund. SJM notes the continuing support of an anonymous Private Foundation. JRC acknowledges the support of the WSU School of Medicine.

Abbreviations List

DI-CMT; Dominant Intermediate Charcot-Marie Tooth Syndrome, DNM2; Dynamin 2, PH; Pleckstrin homology domain, GD; GTPase domain, MD; Middle domain, GED; GTPase effector domain, PRD; Proline rich domain, CNS; Central Nervous System, PNS; Peripheral Nervous System, AP; autophagosome, ATG; Autophagy related gene, TT; Transiently Transfected, NT; Non-Transfected, WT; Wild-Type, SC; Schwann Cell, FBS; Foetal Bovine Serum, PBS, Phosphate Buffered Saline, HRP; Horse-Radish Peroxidase, ECL; Enhanced-Chemiluminescence.; AVO, Acidic Vacuolar Organelle.

References

Cai Y, Arikkath J, Yang L, Guo ML, Periyasamy P, Buch S. Interplay of endoplasmic reticulum stress and autophagy in neurodegenerative disorders. Autophagy. 2016;12(2):225-44.

Churchward, M., Butt, R. H., Lang, J., Hsu, K., Coorssen, J., 2005. Enhanced detergent extraction for analysis of membrane proteomes by two-dimensional gel electrophoresis. Proteome Sci. 3, 5.

Claeys. K.G., Züchner, S., Kennerson. M., Berciano, J., Garcia, A., Verhoeven. K., Storey. E., Merory. J.R., Bienfait. H.M., Lammens. M., Nelis. E., Baets. J., De Vriendt. E., Berneman. Z.N., De Veuster. I., Vance. J.M., Nicholson. G., Timmerman. V. and P. De Jonghe. 2009. Phenotypic spectrum of dynamin 2 mutations in Charcot-Marie-Tooth neuropathy. Brain. 132(7): 1741-1752

Durieux AC, Vassilopoulos S, Lainé J, Fraysse B, Briñas L, Prudhon B, Castells J, Freyssenet D, Bonne G, Guicheney P, Bitoun M. A centronuclear myopathy--dynamin 2 mutation impairs autophagy in mice. Traffic. 2012 Jun;13(6):869-79.

Fang X, Zhou J, Liu W, Duan X, Gala U, Sandoval H, Jaiswal M, Tong C. Dynamin Regulates Autophagy by Modulating Lysosomal Function. J Genet Genomics. 2016 Feb 20;43(2):77-86.

Fergurson, C.J., Lenk. G.M. and M.H. Meisler. 2009. Defective autophagy in neurons and astrocytes from

mice deficient in PI(3,5)P2. Hum. Mol. Genet. 18(24): 4868-4878.

Ferguson S. M., Raimondi A., Paradise S., Shen H., Mesaki K., Ferguson A., Destaing O., Ko G., Takasaki J., Cremona O. et al. (2009). Coordinated actions of actin and BAR proteins upstream of dynamin at endocytic clathrin-coated pits. Dev. Cell 17, 811–822.

Fujita N, Itoh T, Omori H, Fukuda M, Noda T, Yoshimori T. The Atg16L complex specifies the site of LC3 lipidation for membrane biogenesis in autophagy. Mol Biol Cell. 2008 May;19(5):2092-100.

Ghavami, S., Shojaei, S., Yeganeh, B., Ande, S. R., Jangamreddy, J. R., Mehrpour, M., Christoffersson, J., Chaabane, W., Moghadam, A. R., Kashani, H. H., Hashemi, M., Owji, A. A. & Los, M. J. 2014. Autophagy and apoptosis dysfunction in neurodegenerative disorders. Prog Neurobiol, 112, 24-49.

H. Skre. 1974. Genetic and clinical aspects of Charcot-Marie-Tooth's disease. Clinical Genetics. 6: 98-118

Jaeger, P.A. and T. Wyss-Coray. 2009. All-you-can-eat: autophagy in neurodegeneration and neuroprotection. Mol. Neurodegener. 4:16.

Kang. R., Zeh. HJ., Lotze. MT. and D. Tang. 2011. The Beclin 1 network regulates autophagy and apoptosis. Cell. Death. Differ. 18: 571-580.

Kirkin V, McEwan DG, Novak I, Dikic I. A role for ubiquitin in selective autophagy. Mol Cell. 2009 May 15;34(3):259-69.

Krista M. Hennig, Julien Colombani, Thomas P. Neufeld, TOR coordinates bulk and targeted endocytosis in the Drosophila melanogaster fat body to regulate cell growth, J Cell Biol. 2006. 173(6): 963–974.

Klinosky. D.J., Cregg. J.M., Dunn. W.A Jr., Emr. S.D., Sakai. Y., Sandoval. I.V., Sibirny. A., Subramani. S., Thumm. M., Veenhuis. M. and Y. Ohsumi. 2003. A unified nomenclature for yeast autophagy-related genes. Dev. Cell. 5(4): 539-545

Koch, J.C., Knöferle. J., Tönges, L., Ostendorf, T., Bähr. M. and P. Lingor. 2010. Acute axonal degeneration in vivo is attenuated by inhibition of autophagy in a calcium-dependant manner. Autophagy. 6(5): 658-659

Kumar R, Azam S, Sullivan JM, Owen C, Cavener DR, Zhang P, Ron D, Harding HP, Chen JJ, Han A, White BC, Krause GS, DeGracia DJ. Brain ischemia and reperfusion activates the eukaryotic initiation factor 2alpha kinase, PERK. J Neurochem. 2001 Jun;77(5):1418-21.

Lee, S.M., Olzmann, J.A., Chin, LS. and L. Li. 2011. Mutations associated with Charcot-Marie-Tooth disease cause SIMPLE protein mislocalization and degradation by the proteasome and aggresome-autophagy pathways. J. Cell. Sci. 124(19): 3319-3331.

Liu. L., Zhang, R,. 2014. Intermediate Charcot-Marie-Tooth disease. Neurosci Bull. 30(6): 999-1009.

Malhotra JD1, Kaufman RJ. ER stress and its functional link to mitochondria: role in cell survival and death. Cold Spring Harb Perspect Biol. 2011 Sep 1;3(9).

McNiven. M.A., Cao. H., Pitts. K.R. and Y.Yoon. 2000. The dynamin family of mechanoenzymes: pinching in new places. Trends. Biochem. Sci. 25(3): 115-120.

Nixon RA, The role of autophagy in neurodegenerative disease, Nat Med. 2013 Aug;19(8):983-97.

Praefcke. G.J. and H.T. McMahon. 2004. The dynamin superfamily: universal membrane tubulation and fission molecules? Nat. Rev. Mol. Cell. Biol. 5(2): 133-147.

Ramachandran. R. 2010. Vesicle scission: dynamin. Semin. Cell. Dev. Biol. 22(1): 10-17

Rangarajy, S., Verrier, J.D., Madorsky, I., Nicks, J., Dunn Jr, W.A. and L. Notterpek. 2010. Rapamycin Activated Autophagy and Improves Myelination in Explant Cultures from Neuropathic Mice. J. Neurosci. 30(34): 11388-11397

Shang L, Chen S, Du F, Li S, Zhao L, Wang X. Nutrient starvation elicits an acute autophagic response mediated by Ulk1 dephosphorylation and its subsequent dissociation from AMPK. Proc Natl Acad Sci U S A. 2011 Mar 22;108(12):4788-93.

Smith PK, Krohn RI, Hermanson GT, Mallia AK, Gartner FH, Provenzano MD, et al. Measurement of protein using bicinchoninic acid. Anal Biochem. 1985;150:76–85.

Stimpson, SE, Coorssen, JR. Myers, SJ. 2014. Mitochondrial protein alterations in a familial peripheral neuropathy caused by mutations in the sphingolipid protein, SPTLC1. J Chem Biol. Doi: 10.1007/s12154-014-0125-x

Wu, J., Dang. Y., Su. W., Liu. C., Ma. H., Shan. Y., Pei. Y., Wan. B., Guo. J. and L. Yu. 2006. Molecular cloning and characterization of rat LC3A and LC3B - Two novel markers of autophagosome. Biochim. Biophys. Acta. 339(1): 437-442.

Yin Y, Sun G, Li E, Kiselyov K, Sun D, ER stress and impaired autophagy flux in neuronal degeneration and brain injury. Ageing Res Rev. 2016 Sep 1. pii: S1568-1637(16)30169-6. doi: 10.1016/j.arr.2016.08.008. Epub ahead of print

Yorimitsu. T. and D.J. Klinosky. 2005. Autophagy:

molecular machinery for self-eating. Cell. Death. Differ. 12(2): 1542-1552

Yue, Z., Friedman. L., Komatsu. M. and K. Tanaka. 2009. The cellular pathways of neuronal autophagy and their implication in neurodegenerative diseases. Biochim. Biophys. Acta. 1793(9): 1496-1507.

Zuchner. S., Noureddine. M., Kennerson. M., Verhoeven. K., Claeys. K., Jonghe. P.D., Merory. J., Oliveira. S.A., Speer. M.C., Stenger. J.E., Walizada. G., Zhu. D., Pericak-Vance. M.A., Nicholson G., Timmerman, V. and J.M. Vance. 2005. Mutations in the pleckstrin homology domain of dynamin 2 cause dominant intermediate Charcot-Marie-Tooth disease. Nat. Genet. 37(3): 289-294.

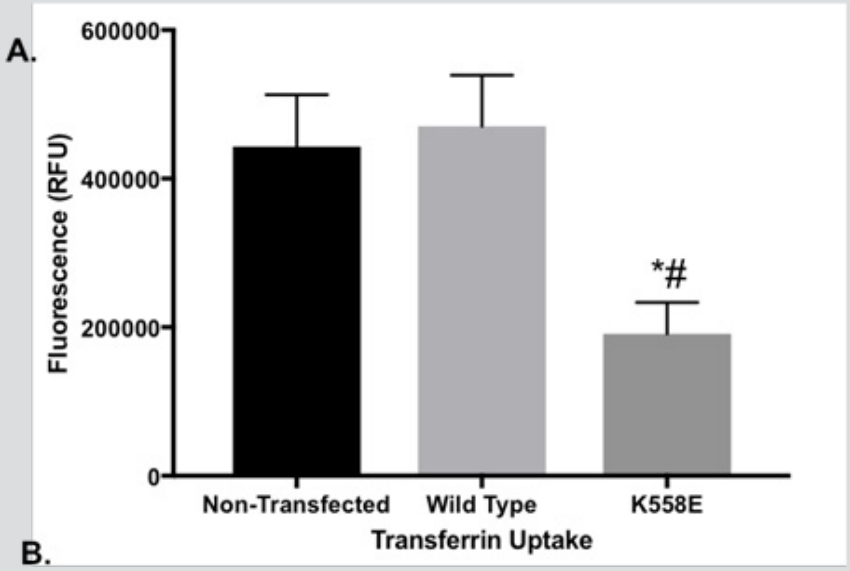

Figure 9: Receptor mediated endocytosis. Uptake of texas-red conjugated transferrin was measured using a fluorescence plate reader and expressed quantitatively (A) and using confocal microscopy (B). K558E mutant shows a significant decrease in RME of transferrin compared to NT * ($p < 0.05$) and WT # ($p < 0.005$) ($n=6$). Representative confocal micrographs showing punctate structures with transferrin-texas red (red), GFP (green) and DAPI nuclear stain (blue). Scale bar = 5 μm.